# Plasmonic absorption enhancement in periodic cross-shaped graphene arrays

**Shaolin Ke,[1] Bing Wang,[1,*] He Huang,[1,2] Hua Long,[1] Kai Wang,[1] and Peixiang Lu[1,2,3]**

[1] *Wuhan National Laboratory for Optoelectronics and School of Physics, Huazhong University of Science and Technology, Wuhan 430074, China*
[2] *School of Science, Wuhan Institute of Technology, Wuhan 430205, China*
[3] *lupeixiang@hust.edu.cn*
[*] *wangbing@hust.edu.cn*

**Abstract:** We present a wavelength tunable absorber composed of periodically patterned cross-shaped graphene arrays in the far-infrared and THz regions. The absorption of the single-layer array can essentially exceed the continuous graphene sheet by increasing the cross-arm width, even for small graphene filling ratio. As chemical potential and relaxation time increase, the absorption can be significantly enhanced. The complementary structure shows higher absorption compared to the original graphene array. Moreover, the wavelength of absorption maximum is angle-insensitive for both TE and TM polarizations. The absorption efficiency can be further improved with double layers of the cross-shaped graphene arrays, which are helpful to design dual-band and broadband absorbers.



**OCIS codes:** (310.6628) Subwavelength structures, nanostructures; (240.6680) Surface plasmons; (310.3915) Metallic, opaque, and absorbing coatings.

## References and links

1. C. Watts, X. Liu, and W. Padilla, "Metamaterial electromagnetic wave absorbers," Adv. Mater. Weinheim **24**(23), OP98–OP120 (2012).
2. Y. Li, H. Yan, D. Farmer, X. Meng, W. Zhu, R. Osgood, T. Heinz, and P. Avouris, "Graphene plasmon enhanced vibrational sensing of surface-adsorbed layers," Nano Lett. **14**(3), 1573–1577 (2014).
3. S. Thongrattanasiri, F. Koppens, and F. Abajo, "Complete optical absorption in periodically patterned graphene," Phys. Rev. Lett. **108**(4), 047401 (2012).
4. A. Grigorenko, M. Polini, and K. Novoselov, "Graphene plasmonics," Nat. Photonics **6**(11), 749–758 (2012).
5. F. Xia, H. Wang, D. Xiao, M. Dubey, and A. Ramasubramaniam, "Two-dimensional material nanophotonics," Nat. Photonics **8**(12), 899–907 (2014).
6. P. Avouris and M. Freitag, "Graphene photonics, plasmonics, and optoelectronics," IEEE J. Sel. Top. Quantum Electron. **20**(1), 6000112 (2014).
7. F. Javier, G. Abajo, "Graphene plasmonics: challenges and opportunities," ACS Photon. **1**(3), 135–152 (2014).
8. B. Wang, X. Zhang, X. Yuan, and J. Teng, "Optical coupling of surface plasmons between graphene sheets," Appl. Phys. Lett. **100**(13), 131111 (2012).
9. B. Wang, H. Huang, K. Wang, H. Long, and P. Lu, "Plasmonic routing in aperiodic graphene sheet arrays," Opt. Lett. **39**(16), 4867–4870 (2014).
10. K. Novoselov, V. Falko, L. Colombo, P. Gellert, M. Schwab, and K. Kim, "A roadmap for graphene," Nature **490**(7419), 192–200 (2012).
11. D. Wang, X. Liu, L. He, Y. Yin, D. Wu, and J. Shi, "Manipulating graphene mobility and charge neutral point with ligand-bound nanoparticles as charge reservoir," Nano Lett. **10**(12), 4989–4993 (2010).
12. G. Pirruccio, L. Moreno, G. Lozano, and J. Rivas, "Coherent and broadband enhanced optical absorption in graphene," ACS Nano **7**(6), 4810–4817 (2013).

#233830 - $15.00 USD Received 5 Feb 2015; revised 20 Mar 2015; accepted 20 Mar 2015; published 30 Mar 2015

13. Z. Fang, Y. Wang, A. Schlather, Z. Liu, P. Ajayan, F. Abajo, P. Nordlander, X. Zhu, and N. Halas, "Active tunable absorption enhancement with graphene nanodisk arrays," Nano Lett. **14**(1), 299–304 (2014).
14. K. Mak, M. Sfeir, Y. Wu, C. Lui, J. Misewich, and T. Heinz, "Measurement of the optical conductivity of graphene," Phys. Rev. Lett. **101**(19), 196405 (2008).
15. A. Nikitin, F. Guinea, and L. Martin-Moreno,"Resonant plasmonic effects in periodic graphene antidot arrays," Appl. Phys. Lett. **101**(15), 151119 (2012).
16. A. Ferreira, N. Peres, R. Ribeiro, and T. Stauber, "Graphene-based photodetector with two cavities," Phys. Rev. B **85**(11), 115438 (2012).
17. T. Zhan, F. Zhao, X. Hu, X. Liu, and J. Zi, "Band structure of plasmons and optical absorption enhancement in graphene on subwavelength dielectric gratings at infrared frequencies," Phys. Rev. B **86**(16), 165416 (2012).
18. J. Piper and S. Fan, "Total absorption in a graphene monolayer in the optical regime by critical coupling with a photonic crystal guided resonance," ACS Photon. **1**(4), 347–353 (2014).
19. J.-T. Liu, N.-H. Liu, J. Li, X. Li, and J.-H. Huang, "Enhanced absorption of graphene with one-dimensional photonic crystal," Appl. Phys. Lett. **101**(5), 052104 (2012).
20. C. Qin, B. Wang, H. Huang, H. Long, K. Wang, and P. Lu, "Low-loss plasmonic supermodes in graphene multilayers," Opt. Express **22**(21), 25324–25332 (2014).
21. X. Meng, R.Grote, J. Dadap, N. Panoiu, and R. Osgood, " Engineering metal-nanoantennae/dye complexes for maximum fluorescence enhancement," Opt. Express **22**(18), 22018–22030 (2014).
22. J. Luo, Y. Li, Z. Wang, Q. Zhang and P. Lu, "Ultra-short isolated attosecond emission in mid-infrared inhomogeneous fields without CEP stabilization," J. Phys. B **46**, 145602 (2013).
23. A. Nikitin, F. Guinea, F. Garcła-Vidal, and L. Martłn-Moreno, "Edge and waveguide terahertz surface plasmon modes in graphene microribbons," Phys. Rev. B **84**(16), 161407 (2011).
24. L. Ju, B. Geng, J. Horng, C. Girit, M. Martin, Z. Hao, H. Bechtel, X. Liang, A. Zettl, Y. Shen, and F. Wang, "Graphene plasmonics for tunable terahertz metamaterials," Nat. Nanotechnol. **6**(10), 630–634 (2011).
25. A. Nikitin, F. Guinea, F. Garcia-Vidal, and L. Martin-Moreno, "Surface plasmon enhanced absorption and suppressed transmission in periodic arrays of graphene ribbons," Phys. Rev. B **85**(8), 081405 (2012).
26. A. Fallahi and J. Perruisseau-Carrier, "Design of tunable biperiodic graphene metasurfaces," Phys. Rev. B **86**(19), 195408 (2012).
27. A. Andryieuski and A. Lavrinenko, "Graphene metamaterials based tunable terahertz absorber: effective surface conductivity approach," Opt. Express **21**(7), 9144–9155 (2013).
28. R. Alaee, M. Farhat, C. Rockstuhl, and F. Lederer, "A perfect absorber made of a graphene micro-ribbon metamaterial," Opt. Express **20**(27), 28017–28024 (2012).
29. Y. Zhang, Y. Feng, B. Zhu, J. Zhao, and T. Jiang, "Graphene based tunable metamaterial absorber and polarization modulation in terahertz frequency," Opt. Express **22**(19), 22743–22752, (2014).
30. H. Tao, N. Landy, C. Bingham, X. Zhang, R. Averitt, and W. Padilla, "A metamaterial absorber for the terahertz regime: design, fabrication and characterization," Opt. Express, **16**(10), 7181–7188 (2008).
31. X. Liu, T. Starr, A. Starr, and W. Padilla, "Infrared spatial and frequency selective metamaterial with near-unity absorbance," Phys. Rev. Lett. **104**(20), 207403 (2010).
32. C. Helgert, C. Menzel, C. Rockstuhl, E. Pshenay-Severin, E. Kley, A. Chipouline, A. Tnnermann, F. Lederer, and T. Pertsch, "Polarization-independent negative-index metamaterial in the near infrared," Opt. Lett. **34**(5), 704–706 (2009).
33. D. Shchegolkov, A. Azad, J. OHara, and E. Simakov, "Perfect subwavelength fishnetlike metamaterial-based film terahertz absorbers," Phys. Rev. B **82**(20), 205117 (2010).
34. P. Y. Chen and A. Al, "Atomically thin surface cloak using graphene monolayers," ACS Nano **5**(7), 5855–5863 (2011).
35. X.-H. Deng, J.-T. Liu, J. Yuan, T.-B. Wang, and N.-H. Liu, "Tunable THz absorption in graphene-based heterostructures," Opt. Express **22**(24), 30177–30183 (2014).
36. G.W. Hanson, "Quasi-transverse electromagnetic modes supported by a graphene parallel-plate waveguide," J. Appl. Phys **104**(8), 084314 (2008).
37. B. Wang, X. Zhang, K. Loh, and J. Teng, "Tunable broadband transmission and phase modulation of light through graphene multilayers," J. Appl. Phys. **115**(21), 213102 (2014).
38. Y. Ye, Y. Jin, and S. He, "Omnidirectional, polarization-insensitive and broadband thin absorber in the terahertz regime," J. Opt. Soc. Am. B **27**(3), 498–504 (2010).
39. H. Yan, X. Li, B. Chandra, G. Tulevski, Y. Wu, M. Freitag, W. Zhu, P. Avouris, and F. Xia, "Tunable infrared plasmonic devices using graphene/insulator stacks," Nat. Nanotechnol. **7**(5), 330–334 (2012).
40. Y. Cui, K. Fung, J. Xu, H. Ma, Y. Jin, S. He, and N. Fang, "Ultrabroadband light absorption by a sawtooth anisotropic metamaterial slab," Nano Lett. **12**(3), 1443–1447 (2012).

#233830 - $15.00 USD Received 5 Feb 2015; revised 20 Mar 2015; accepted 20 Mar 2015; published 30 Mar 2015

## 1. Introduction

Efficient light harvest and absorption have attracted much attention in recent years in virtue of the promising applications in emitters, solar photovoltaics, sensors, and spatial light modulators [1, 2]. The emergence of many exotic materials has stimulated the proposal of new-type absorbers. For example, the complete light absorption has been theoretically demonstrated by using patterned graphene resonators [3]. Graphene is a two-dimensional material and manifests quite a few fantastic optical properties thanks to its unique electronic band structures [4–9]. Graphene based absorbers have advantages of continuously tunable surface conductivity [10]. The high carrier mobility in graphene makes it suitable for ultra-fast switching [11]. As a dimensionless and flexible material, graphene is convenient to integrate with other optical nanodevices [12, 13]. In the visible range, graphene manifests saturate absorption feature. A single sheet of graphene can absorb approximately 2.3% energy of incident light [14, 15]. In order to improve the absorption efficiency, one has incorporated graphene to optical cavities [16], dielectric gratings [17], and photonic crystals [18, 19], where light can be efficiently trapped and absorbed.

In infrared and teraherz(THz) range, graphene behaves like metal when interacting with external light waves and can support surface plasmon polaritons (SPPs) [4,20], which enable huge concentrations of optical energy [21,22]. The SPPs in graphene will benefit to the enhancement of light absorption [23]. Recently, a great diversity of patterned graphene arrays have been proposed and demonstrated in enhancing absorption by take advantage of graphene SPPs, such as graphene discs, ribbons, rings, and cross-shaped structures [3, 15, 24–29]. When the light impinges on graphene, the SPP resonance might occur in the patterns, leading to plasmonic absorption enhancement. The SPP resonance tends to be associated with the generation of leaky modes, resulting in a shift of resonance compared to the absorption cross-section for a single graphene cell [25]. The total absorption has also been predicted in patterned graphene arrays with dielectric substrate. As the total internal reflection occurs at the interface of dielectric and air, the evanescent coupling of incident light to graphene SPPs brings about external absorption. The metallic substrate coated by a dielectric layer may play the same role in absorption enhancement [3].

In this wok, we present a systematical study on plasmonic absorption enhancement in periodic cross-shaped graphene arrays. Cross-shaped resonator is a typical electric ring resonator (ERR) which couples strongly to uniform electric fields, but negligibly to magnetic ones [30, 31]. It shows polarization-independent response for normal incidence due to its $C_4$ symmetry [32, 33]. The proposed structure has the advantage of one more free geometry parameter compared to the graphene disk and ribbon, so the absorption could be tuned more flexibly.

The content of the work is arranged as follows. In Sec. 2, the configuration of the proposed absorber structure is described. We also introduce briefly the method of calculating the absorption spectrum. The dependence of the absorption spectrum on the geometric parameters is discussed in Sec. 3. The situation of oblique incidence for different polarizations is investigated as well. In Sec. 4, the influences of chemical potential and relaxation time on absorption are considered. In addition, the complementary structure and double layers of the cross-shaped graphene patterns are studied in Secs. 5 and 6, respectively. Finally, we draw the conclusion of the whole work in the last section.

## 2. Geometry of the cross-shaped graphene array

Figure 1 schematically depicts the structure of proposed absorber composed of a square cross-shaped graphene array with period $a$, length $L$, and width $w$. The graphene array adheres to a silica substrate separated by a thin silicon dioxide spacer with thickness $d$. The relative per-

#233830 - $15.00 USD Received 5 Feb 2015; revised 20 Mar 2015; accepted 20 Mar 2015; published 30 Mar 2015

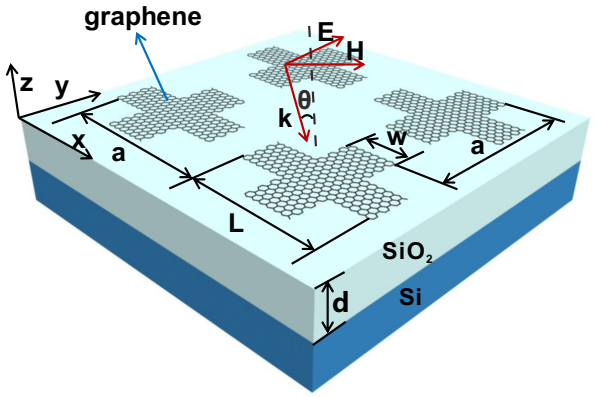


Fig. 1. Schematic of the geometry under consideration: the periodic cross-shaped graphene arrays with width $w$, length $L$ and period $a$. The arrays are supported on a Si substrate coated by a thin $SiO_2$ layer with thickness $d$. The incident electromagnetic wave is TE polarized with the electric fields along the $y$ axis. The angle of incidence is $\theta$.

mittivity of $SiO_2$ is given by $\varepsilon_d = 3.9$ and the refractive index of Si by $n_s$ = 3.4 [34, 35]. The system is illuminated from air by a plane wave with wavelength $\lambda$ and incident angle $\theta$. The incident plane is the $x$-$z$ plane. In practice, the large-area graphene film can be first grown using an optimized liquid precursor chemical vapor deposition method and determined to be single-layer through Raman measurements. The electron-beam lithography is used to pattern the graphene film into cross-shaped structures and the exposed area can be etched away by the oxygen plasma [13].

The surface conductivity of graphene $\sigma$ can be modeled by the Kubo formula including interband and intraband transitions [34]. In the THz and far infrared range, the interband transition dominates and the surface conductivity can be simplified as $\sigma(\omega) = \frac{e^2\mu_c}{\pi\hbar^2}\frac{i}{\omega+i/\tau}$ when $\mu_c \gg k_B T_m$, where $e$, $k_B$, and $\hbar$ are the universal constants representing the electron charge, reduced Planck's constant, and Boltzmanns constant, respectively [36]. $T_m$, $\mu_c$, $\tau$, and $\omega$ are the temperature, chemical potential, relaxation time, and photon frequency, respectively. In this work, the room temperature ($T_m$ = 300 K) is assumed. The chemical potential and relaxation time $\tau = 0.5$ ps and $\mu_c = 0.4$ eV are initially considered and their influences will be analyzed later.

Numerical simulations are performed with the commercial software COMSOL Multiphysics based on finite element method. The graphene is modeled by using the surface current boundary condition [15, 27]. The domain has been discretized by using an inhomogeneous mesh with the maximal element size being less than 10% of graphene surface plasmons wavelength. The transmission $T(\omega) = |S_{21}(\omega)|^2$, reflection $R(\omega) = |S_{11}(\omega)|^2$, and absorption $A(\omega) = 1 - T(\omega) - R(\omega)$ are obtained from $S$-parameters.

## 3. General absorption properties

We first investigate the geometric effects on the absorption of periodic single layer cross-shaped graphene arrays at normal incidence. As the width-to-length ratio $w/L$ and length-to-period ratio $L/a$ of the cross-shaped graphene varies, there is always an evident absorption peak in the far-infrared and THz range. In Fig. 2(a), where the cross-arm length is fixed at $L$ = 1.25 $\mu$m, the results show that, as the arm width increases, the peak first experiences a blueshift and then undergoes a redshift, while the absorption maximum gradually increases at the same time. It is

#233830 - $15.00 USD Received 5 Feb 2015; revised 20 Mar 2015; accepted 20 Mar 2015; published 30 Mar 2015

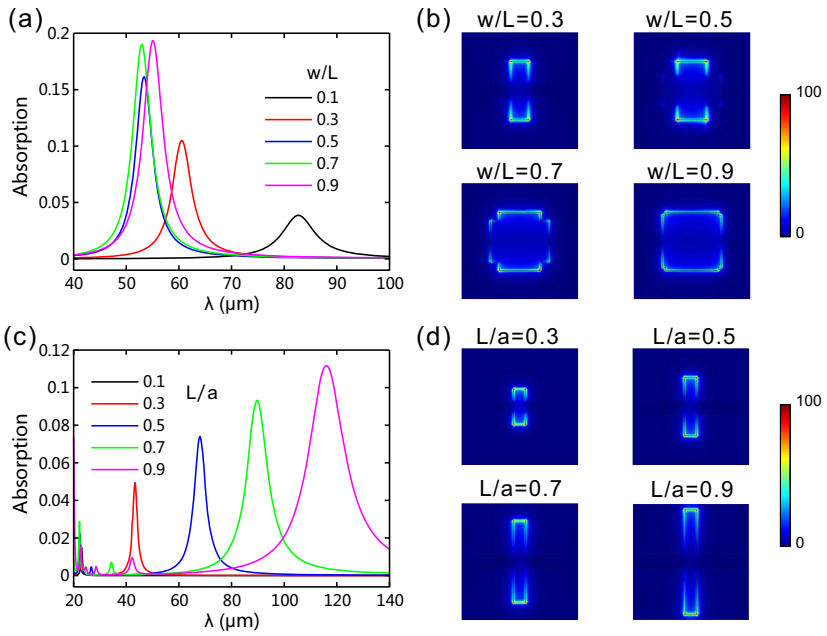


Fig. 2. (a) The absorption spectra for different widths as $L$ = 1.25 $\mu$m. (b)The electric field distributions ($|\mathbf{E}|$) at the absorption peak for $w/L$ = 0.3, 0.5, 0.7, and 0.9. (c) The absorption spectra for different lengths as $w$ = 0.25 $\mu$m. (d) The electric field distributions at the absorption peak for $L/a$ = 0.3, 0.5, 0.7, and 0.9. $a$ = 2.5 $\mu$m and $d$ = 0.3 $\mu$m.

also apparent that the absorption peak broadens in longer wavelength. The absorption maximum occurs when the SPPs are resonating mainly in the vertical arms and the resonance condition reads $2k_{sp}L + 2\delta = 2p\pi$, where $k_{sp} = 2\pi n_{sp}/\lambda_m$ with $n_{sp}$ being the effective index of SPPs and $\lambda_m$ the resonance wavelength. The phase change at the ends of the arm is denotes by $\delta$ and $p$ is an integer. As the incident wavelength is much larger than the arm length, we can suppose $p = 1$. Therefore, the resonant wavelength is given by $\lambda_m = 2\pi n_{sp}L/(\pi - \delta)$. The effective index of SPPs $n_{sp}$ depends largely on the width of arm. As $w \ll L$, the narrower graphene strip suggests larger $n_{sp}$ [23]. As a result, the resonance peak experiences a blue shift as $w$ increases when $w$ is small. On the other hand, when $w$ approaches to $L$, the SPP resonance in the horizontal arms cannot be neglected. The resonant wavelength in the horizontal arm increases as $w$ increases since the cavity length increases. To some extent, the resulted resonant wavelength may undergo a slight redshift. The reason for the absorption peak broadens at longer wavelengths lies in the fact that the real part of the surface conductivity of graphene increases at longer wavelengths [37],arousing additional propagation loss of SPPs. Therefore, the Q-factor of SPPs resonating in the cross is damping. Since here $L$ = 1.25 $\mu m$ and $a$ = 2.5 $\mu m$, the area ratio of graphene in a unit cell is smaller than 0.25 as $w$ varies. The absorption maximum can reach 0.18 for wide cross arms, essentially exceeding 2.3% absorption in continuous monolayer graphene. As $w/L$ approaches to unity, the configuration gradually transforms to be a square. In this case, the absorption of the square-shaped graphene array might be comparable with the cross-shaped one or even higher. Nevertheless, the cross-shaped arrays have an additional degree of freedom in geometry. As the width of the two arms could vary independently, the cross configuration is

#233830 - $15.00 USD Received 5 Feb 2015; revised 20 Mar 2015; accepted 20 Mar 2015; published 30 Mar 2015

applicable to design omnidirectional and polarization-independent absorbers [38].

The electric field distributions ($|\mathbf{E}|$) at the absorption peak for different widths are illustrated in Fig. 2(b). It is shown that a strong localization of electromagnetic fields can be realized and the fields concentrate mostly on the edges of cross-arm. The localization is caused by the strong electric dipole resonances, which result from the charges accumulated at the edges of cross-arm. Such strong resonances effectively trap light energy and provide sufficient time to dissipate it by the Ohmic losses within the graphene. The electric fields are well confined in the cross-arm along the $y$ axis for $w/L$ = 0.3. As arm width increases, the electric fields gradually couple to the arm along the $x$ axis due to the enhancement of resonance in the horizontal arms. Figure 2(c) shows the influences of cross-arm length on the absorption spectra, in which the width is fixed at $w$ = 0.25 $\mu$m. The variation of resonant wavelength with the change of length is more evident than width. As $L$ increases, the resonant wavelength shifts from 23 $\mu$m to 116 $\mu$m and absorption maximum increases from 0.015 to 0.11. The fields always concentrate at the edges of the longitude arms as shown in Fig. 2(d), indicating the cross-shaped resonator couples strongly to the electric fields. The effective index of SPPs $n_{sp}$ depends largely on the width of arm and the narrower graphene strip suggests larger $n_{sp}$. In the case of $y$-polarization, as $w \ll L$, the vertical arm suggests larger $n_{sp}$ than the horizontal arm. Light trends to concentrate on the media with larger index, resulting in the absence of field along the horizontal arm.

In Figure 3, the resonant wavelength $\lambda_m$ and the absorption maximum $A_m$ as a function of the length-to-period ratio $L/a$ and width-to-length ratio $w/L$ are depicted. The period is set as $a = 2.5$ $\mu$m for Figs. 3(a) and 3(b). As displayed in Fig. 3(a), for a fixed width-to-length ratio, the resonant wavelength increases monotonically as $L/a$ increases. As $L/a$ is fixed, the resonant wavelength decreases when $w/L$ varies from 0.1 to 0.6 and then increases slightly as

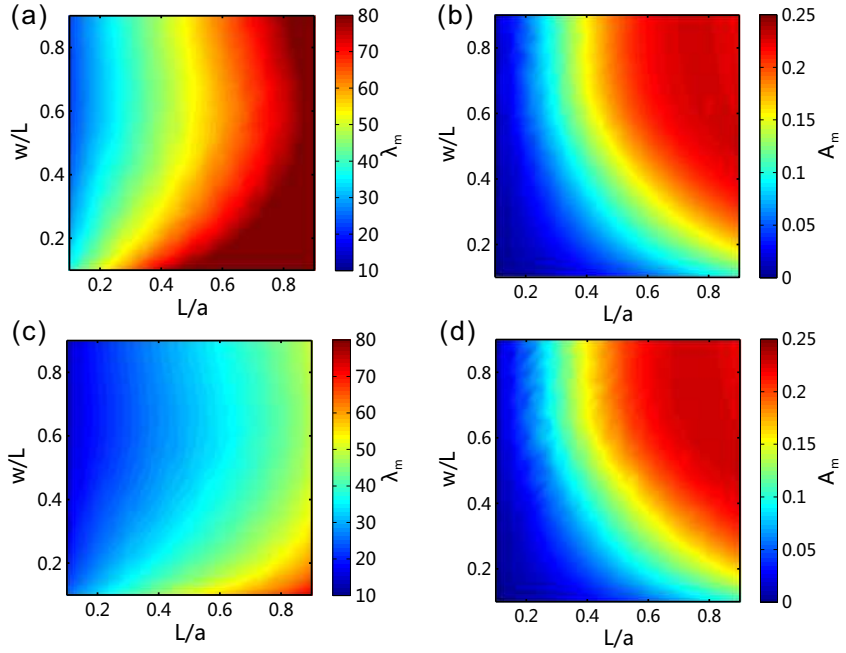


Fig. 3. The resonant wavelength $\lambda_m$ and the absorption maximum $A_m$ as a function of $L/a$ and $w/L$ for different periods. The resonant wavelength for (a) $a$ = 2.5 $\mu$m and (c) $a$ = 1.0 $\mu$m. The absorption maximum for (b) $a$ = 2.5 $\mu$m and (d) $a$ = 1.0 $\mu$m. In all panels, $d$ = 0.3 $\mu$m.

#233830 - $15.00 USD Received 5 Feb 2015; revised 20 Mar 2015; accepted 20 Mar 2015; published 30 Mar 2015

$w/L$ further increases. The minimum resonant wavelength for a fixed cross-arm length will be obtained around $w/L = 0.6$. In Fig. 3(b), the variation of absorption maximum $A_m$ corresponding to resonant wavelength is illustrated. The results show that the absorption of proposed absorber can be enhanced as high as 0.22 when length-to-period ratio is larger than 0.6 by adjusting $w/L$. When $L/a$ is smaller than 0.6, the absorption can be improved to its maximum but less than 0.22 by applying proper width-to-length ratio. The variation of $A_m$ is demonstrated in detail as follows. For a fixed width-to-length ratio, the maximum absorption increases with increasing $L/a$ before reaching its maximum. For large width-to-length ratio, $A_m$ saturates more quickly compared to that for small $w/L$. For a fixed length-to-period, the variation of $A_m$ is similar to that for a fixed width-to-length ratio. Note that the maximum absorption is not located exactly at $w/L = L/a = 1$ in our calculations. As $w/L$ and $L/a$ approach to unity while the graphene sheet is still not continuous, the localized SPP resonance could occur and the absorption peak is remarkably stronger than that of a continuous graphene sheet. The same behavior takes place for other values of the period. For an example, the case $a = 1$ $\mu$m is displayed in Figs. 3(c) and 3(d). Figure 3(c) are similar to that for $a = 2.5$ $\mu$m while the resonant wavelength experiences a blueshift. The dependence of absorption maximum on the geometric parameters is almost unchanged as the period varies.

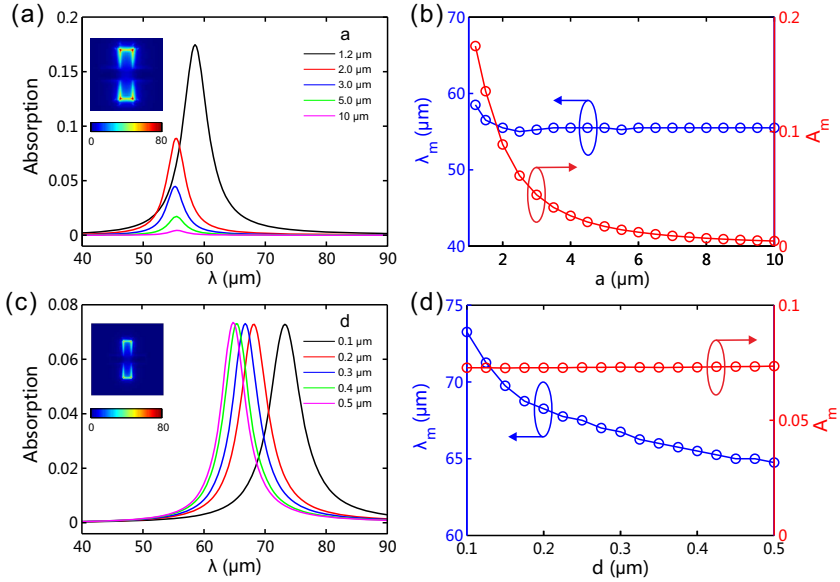


Fig. 4. (a) The absorption spectra for different periods. (b) Dependence of the resonant wavelength and absorption maximum on the period. In (a) and (b), $L = 1$ $\mu$m, $w = 0.25$ $\mu$m, and $d = 0.3$ $\mu$m. (c) The absorption spectra for different thicknesses. (d) Dependence of the resonant wavelength and absorption maximum on thickness. In (c) and (d), $L = 1.25$ $\mu$m, $w = 0.25$ $\mu$m, and $a = 2.5$ $\mu$m. The insert shows electric field distributions ($|\mathbf{E}|$) for (a) $L/a = 0.1$ and (c) $d = 0.1$ $\mu$m.

Figure 4(a) plots the absorption spectra for various periods. It is apparent that the period has a great influence on the absorption maximum but less on the wavelength. The resonant wavelength and the absorption maximum for different periods are displayed in Fig. 4(b). It shows that the resonant wavelength first decreases and then hovers around 55 $\mu$m as period $a$ increases. At the same time, the absorption maximum decreases. The reasons are as follows. As the period increases, the resonant wavelength almost keeps unchanged because the resonance

#233830 - $15.00 USD Received 5 Feb 2015; revised 20 Mar 2015; accepted 20 Mar 2015; published 30 Mar 2015

condition does not change much. Only the filling factor of graphene decreases, leading to the decrease of absorption. The resonant wavelength experiences slight variation at small periods due to the coupling of adjacent graphene crosses. As the period varies, the electric fields always confine at the edges of the longitude arms as shown in the insert of Fig. 4(a).

When the thickness $d$ of the thin $SiO_2$ layer changes, as shown in Figs. 4(c) and 4(d), the resonant wavelength undergoes a blueshift while the absorption maximum almost keeps at 7.3%. When $d > 0.4\ \mu$m, the resonant wavelength is quite stable at $\lambda = 65\ \mu$m. The shift of resonance is related to the change of SPPs wavevector for altering the dielectric environment [15]. The electric field distributions ($|\mathbf{E}|$) are almost unchanged with the thickness increases as shown in the insert of Fig. 4(c).

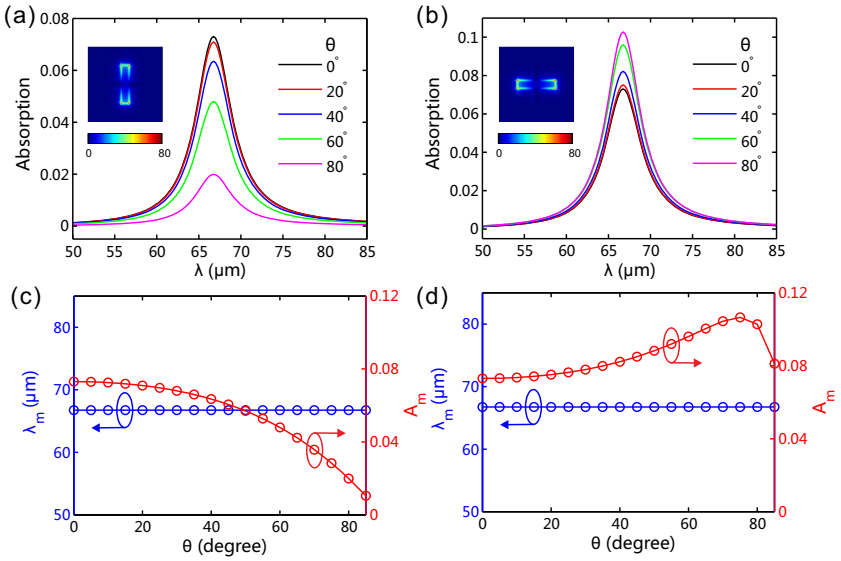


Fig. 5. The absorption spectra at various incident angles for (a) TE and (b) TM polarizations. The resonant wavelength and absorption maximum at various incident angles for (c) TE and (d) TM polarizations. The insert shows the electric field distributions ($|\mathbf{E}|$) at $\theta = 0^\circ$.

The dependencies of the absorption spectra on polarizations are shown in Fig. 5 for different incident angles. The other parameters are chosen as $a = 2.5\ \mu$m, $L = 1.25\ \mu$m, $w = 0.25\ \mu$m, and $d = 0.3\ \mu$m. For both TE and TM polarizations, the resonant wavelength is insensitive to the incident angle, which influences much on the absorption intensity. For TE polarization, the absorption maximum decreases as the incident angle $\theta$ increases. For TM polarization, however, the absorption maximum increases firstly when $\theta$ increases and then undergoes a decline. The reason lies in the increasing reflection of light at highly oblique incidence. The insert in Figs. 5(a) and 5(b) show the electric field distributions ($|\mathbf{E}|$) at the absorption peak for TE and TM polarizations, respectively. The results show that the fields are confined in different arms but along the direction of incident electric fields.

## 4. Influence of graphene optical properties

The surface conductivity of graphene relates largely to the chemical potential $\mu_c$, which can be controlled by electrostatic and chemical doping [13,39]. Figure 6(a) plots the absorption spectra for different values of $\mu_c$ at normal incidence. The geometric parameters are the same with those used in Fig. 5. When the chemical potential changes from 0.1 eV to 0.9 eV, the absorption peak

#233830 - $15.00 USD Received 5 Feb 2015; revised 20 Mar 2015; accepted 20 Mar 2015; published 30 Mar 2015

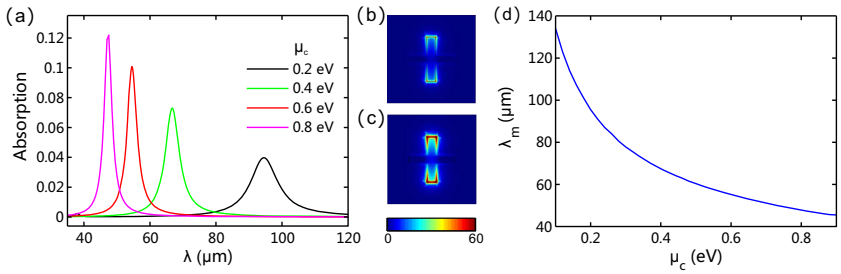


Fig. 6. (a) The absorption spectra for different chemical potentials. (b) and (c) The electric field distributions (|**E**|) at the absorption peak for $\mu_c$ = 0.2 eV and 0.8 eV. (d) The resonant wavelength $\lambda_m$ as a function of $\mu_c$.

experiences a blueshift and the absorption maximum increases simultaneously. The absorption enhancement can be understood as follows. For higher $\mu_c$, the resonance shifts to a less absorptive frequency region and the number of charge carriers contributed to the plasmonic oscillation increases. As a result, the absorption maximum increases. The confined electric fields for high chemical potential are stronger than the low one as shown in Figs. 6(b) and 6(c). The stronger localized fields lead to higher absorption. Figure 6(d) illustrates the resonant wavelength as a function of chemical potential. The results show that $\lambda_m$ decreases monotonously as $\mu_c$ increases. So the resonant wavelength can be tuned by controlling the chemical potential without changing the absorber geometries.

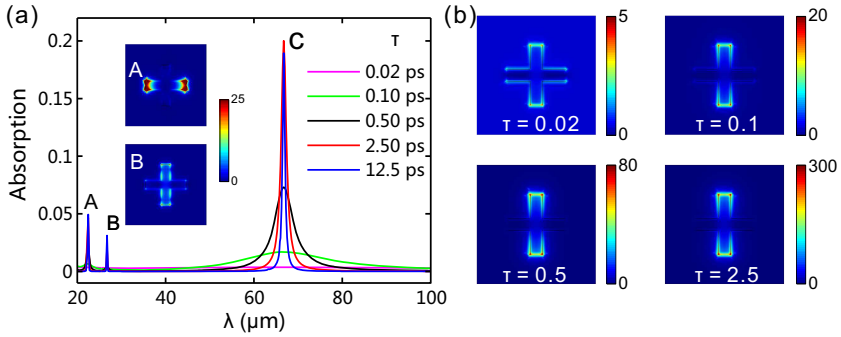


Fig. 7. (a) The absorption spectra for different relaxation times. The insert shows the electric field distributions (|**E**|) for $\tau$ = 0.5 ps at the absorption peaks labeled with A and B. (b) The electric field distributions at the absorption peaks of C for $\tau$ = 0.02 ps, 0.1 ps, 0.5 ps, and 2.5 ps.

The absorption is also associated with the relaxation time of electrons in graphene, which is governed by $\tau = \mu_c \mu/(ev_F^2)$ with $e$ being the electron charge, $v_F = 10^6$ m/s the Fermi velocity, and $\mu$ the carrier mobility. Thus the relaxation time can be directly controlled by varying the chemical potential via electrostatic and chemical doping. When changing the surrounding environment such as placing organic molecules on graphene, the carrier mobility will be significantly enhanced [11], leading to the increasing of relaxation time. Figure 7(a) shows the absorption spectra for different $\tau$. The other parameters are the same as those used in Fig. 5. The absorption peak labeled with C ($\lambda_m$ = 66.75 $\mu m$) in Fig. 7(a) remains unchanged while the width of peak becomes narrower as $\tau$ increases. The absorption maximum increases at first and then decreases as $\tau$ increases. The reasons are as follows. As the relaxation time increases, the

#233830 - $15.00 USD Received 5 Feb 2015; revised 20 Mar 2015; accepted 20 Mar 2015; published 30 Mar 2015

charge carriers contributed to the plasmonic oscillation increases, leading to higher absorption. When number of charge carriers is large enough, most energy will be reflected. As a result, in Fig. 7(a), the absorption decreases.

The absorption peaks labeled with A ($\lambda_m$ = 22.5 $\mu$m) and B ($\lambda_m$ = 26.75 $\mu$m) in Fig. 7(a) turn to be evident for higher $\tau$. Peak A, B, and C represent different exciting modes, which can be characterized from the electric field distributions. For peak A, the electric fields are confined along the $x$ axis, the direction perpendicular to the incident electric fields. The peak B represents a high-order mode, where the fields are discontinuous along the $y$ arm and stronger than that along the $x$ arm. Figure 7(b) shows the electric field distributions ($|\mathbf{E}|$) for peak C (normalized by each own maximum). The results show that a weak electric fields are along the $x$ axis in spite of strong fields confined to the edges of arm along the $y$ axis due to the arrays couple weakly with the electric fields for small $\tau$ and it disappears as relaxation time increases. For continuous monolayer graphene, the transmission and reflection are given by $T = |\frac{2}{2+\eta_0\sigma\cos\theta}|^2$ and $R = |\frac{\eta_0\sigma\cos\theta}{2+\eta_0\sigma\cos\theta}|^2$, where $\eta_0$ is impedance of air. In case of normal incidence, the absorption is given by $A = 1-T-R = \frac{4\eta_0 \mathrm{Re}(\sigma)}{|2+\eta_0\sigma|^2}$. In the visible range, $\sigma$ is almost a constant, resulting the 2.3% absorption. In the THz and far infrared range, $\sigma$ varies with $\tau$. At $\lambda = 66.75$ $\mu m$, $A$ is 3.9% for $\tau = 0.5$ ps and 0.8% for $\tau = 2.5$ ps, which is remarkable lower than that for the patterned graphene. The maximum absorption predicted for the thin layer is 0.5 in the symmetric dielectric environment [3]. By choosing large relaxation time, the absorption induced by the SPPs increases and the maximum absorption is likely to approach the predicted value by carefully adjusting the geometric parameters and the dielectric environment.

## 5. Absorption properties of complementary structures

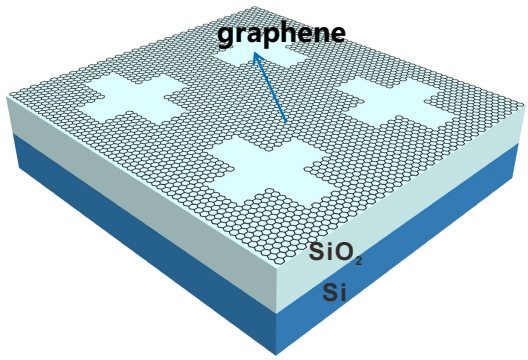


Fig. 8. The complementary structure of Fig. 1.

We also propose the complementary of the periodically patterned cross-shaped graphene arrays. In Fig. 8, the graphene layer is continuous so that the current can pass through directly, because electric transport is required for many devices. The geometric parameters are chosen as $a$ = 2.5 $\mu$m, $L$ = 1.25 $\mu$m, $w$ = 0.25 $\mu$m, and $d$ = 0.3 $\mu$m.

The absorption spectra at various incident angles for TE and TM polarizations are illustrated in Fig. 9. It shows that two more visible resonances at $\lambda$ = 23.75 $\mu m$ (labeled with A) and 36.75 $\mu m$ (labeled with B) in Fig. 9(a) appear visually besides the largest absorption resonant peak. Now we focus on the largest absorption peak at 58.75 $\mu m$ (labeled with C) in Fig. 9(a). The

#233830 - $15.00 USD Received 5 Feb 2015; revised 20 Mar 2015; accepted 20 Mar 2015; published 30 Mar 2015

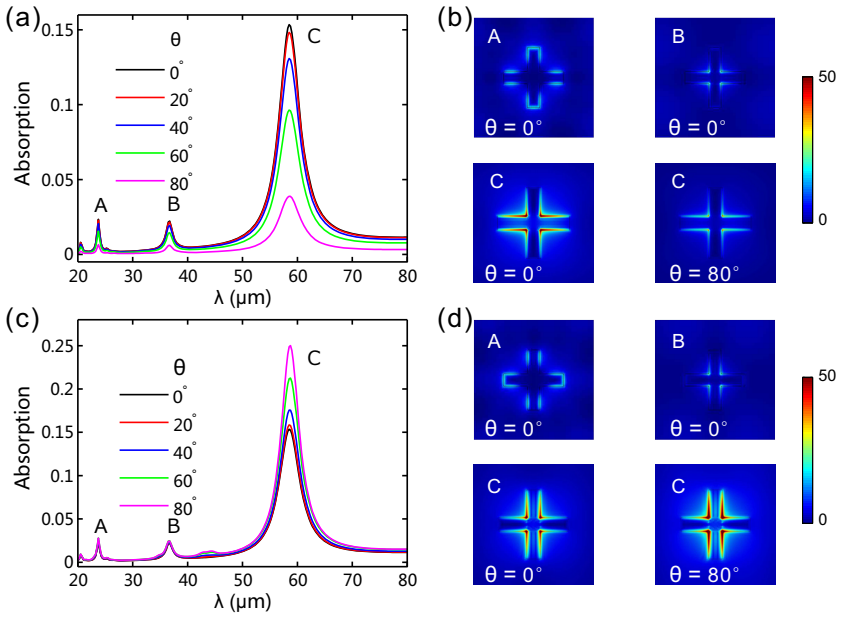


Fig. 9. The absorption spectra at various incident angles for (a) TE and (c) TM polarizations. (b) and (d) The electric field distributions ($|\mathbf{E}|$) at the absorption peak.

absorption behaviors of the complementary structure for incident angles are similar to the cross-shaped one. The resonant wavelength remains unchanged as $\theta$ increases for both polarizations. The absorption maximum decreases for TE polarization while increases for TM polarization as incident angle increases.

The electric field distributions ($|\mathbf{E}|$) for TE polarization are presented in Fig. 9(b). The different distributions of electric fields represent different resonant modes. For peak C, the localized electric fields mainly concentrate on the corners of the cross-arms. The electric field distributions for TM polarization are perpendicular to those for TE. The behaviors of absorption maximum for different polarizations can be understood by the electric field distributions. For TE polarization, the localized electric fields labeled with C as $\theta = 80^\circ$ are weaker than that as $\theta = 0^\circ$, while the situation changes for TM polarization. Stronger confined electric fields lead to higher absorption enhancement.

## 6. Double-layer graphene arrays

The absorption can be further enhanced by applying multilayer graphene arrays [40]. For an example, the absorption for double layers of periodic cross-shaped graphene arrays is studied. Figure 10(a) depicts the structure composed of double layers of graphene arrays separated by $SiO_2$ layer with thickness $h$. The other parameters are $a$ = 2.5 $\mu$m, $L$ = 1.25 $\mu$m, $w$ = 0.25 $\mu$m, and $d$ = 0.3 $\mu$m. Figure 10(b) illustrates the absorption spectra for different $h$. The results show that two absorption bands can be observed. The absorption maximum at short wavelength band exceeds that for single layer graphene arrays with the same parameters and is larger than that in long wavelength band. The resonances for the two band are different for varying $h$. For band of short wavelength, the resonant wavelength experiences a redshift and the absorption maximum decreases as $h$ increases. For long wavelength band, the peak undergoes a blueshift and the absorption maximum increases as $h$ increases. As the distance between the two graphene arrays decreases, the coupling of them becomes stronger. As a result, the mode of individual

#233830 - $15.00 USD Received 5 Feb 2015; revised 20 Mar 2015; accepted 20 Mar 2015; published 30 Mar 2015

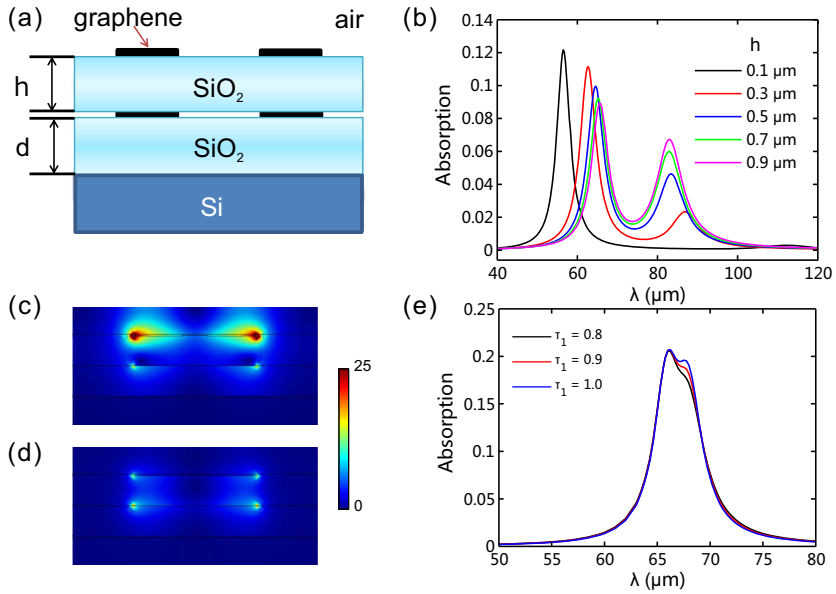


Fig. 10. (a) The structure consisting of double layers of periodic cross-shaped graphene arrays. (b) The absorption spectra for different $h$. (c) and (d) The electric field distributions ($|\mathbf{E}|$) of $y$-$z$ plane across the center as $h$ = 0.3 $\mu$m. (c) $\lambda$ = 62.75 $\mu$m. (d) $\lambda$ = 86.75 $\mu$m. (e) The absorption spectra by applying different chemical potentials for graphene layers as $h$ = 1.6 $\mu$m. $\mu_c$ = 0.4 eV for up layer and $\mu_c$ = 0.6 eV for down layer. The relaxation time for down layer is $\tau_1$ and up layer is 1.0 ps.

plasmon modes in each graphene array splits into two modes because of the symmetric and anti-symmetric coupling. The stronger coupling tends to result in larger splitting of the modes. Figures 10(b)-10(c) show the electric field distributions ($|\mathbf{E}|$) for $h$ = 0.3 $\mu$m. As $\lambda$ = 62.75 $\mu$m, the confined field for upper layer is stronger than that for the down layer while the situation is in reverse as $\lambda$ = 86.75 $\mu$m. This represents different resonant modes. By adjusting the size and applying different chemical potentials for different layers to make the two absorption bands sufficiently close, the two peaks can merge to form a broader absorption band. In Fig. 10(e), a broadband absorption is realized by applying different $\mu_c$ for two layers. So the multilayer graphene arrays are helpful to build multispectral and broadband absorbers [38]. Due to the different Coulomp scattering, the mobility of electrons in graphene could be different in different surrounding environment. We have considered the different relaxation times in Fig. 10(e). The relaxation time has effect on the absorption intensity and Q-factor of the absorption peaks. In practice, the chemical potential of graphene can be tuned independently by performing different doping or add distinct gate voltages. Additionally, the relaxation time of graphene can be tuned by placing organic molecules to pristine graphene.

## 7. Conclusions

In conclusion, we have studied the tunable absorption enhancement in periodic cross-shaped graphene arrays in the aid of SPP resonance. As the width of cross-arm increases, the absorption is getting stronger even for small graphene filling ratio. The absorbtion peak experiences a blueshift at first and then redshift as the width increases. By applying larger chemical potential and relaxation time of graphene, the absorption can be further enhanced. For both TE and

#233830 - $15.00 USD Received 5 Feb 2015; revised 20 Mar 2015; accepted 20 Mar 2015; published 30 Mar 2015

TM polarizations, the absorption wavelength is insensitive to the incident angle, while the absorption maximum behaves differently for distinct polarizations. We have also considered the complementary structure of the cross-shaped arrays, the absorption may be further enhanced and it appears more absorption peaks due to the excitation of higher order modes. Additionally, double-layer graphene arrays may bring about more absorption of incident light and can realize dual-band plasmonic absorption, which will benefit to constructing broadband graphene absorbers.

**Acknowledgment**

This work is supported by the 973 Program (No. 2014CB921301), the National Natural Science Foundation of China (Nos. 11304108 and 11104095), and the Specialized Research Fund for the Doctoral Program of Higher Education of China (No. 20130142120091). Numerical simulations presented in this paper were carried out using the High Performance Computing Center experimental testbed in SCTS/CGCL (see http://grid.hust.edu.cn/hpcc).

#233830 - $15.00 USD Received 5 Feb 2015; revised 20 Mar 2015; accepted 20 Mar 2015; published 30 Mar 2015